International Journal of Naval Architecture and Ocean Engineering 13 (2021) 102–114

Contents lists available at ScienceDirect

International Journal of Naval Architecture and Ocean Engineering

journal homepage: http://www.journals.elsevier.com/international-journal-of-naval-architecture-and-ocean-engineering/

Assessment of the effect of biofilm on the ship hydrodynamic performance by performance prediction method

Andrea Farkas, Nastia Degiuli*, Ivana Martić

Faculty of Mechanical Engineering and Naval Architecture, University of Zagreb, Ivana Lučića 5, Zagreb, 10000, Croatia

ARTICLE INFO

Article history:
Received 12 November 2020
Received in revised form
21 December 2020
Accepted 30 December 2020
Available online 5 March 2021

Keywords:
Biofouling
Ship
Performance prediction
Computational Fluid Dynamics (CFD)
Hydrodynamic characteristics

ABSTRACT

Biofouling represents an important problem in the shipping industry since it causes the increase in surface roughness. The most of ships in the current world fleet do not have good coating condition which represents an important problem due to strict rules regarding ship energy efficiency. Therefore, the importance of the control and management of the hull and propeller fouling is highlighted by the International Maritime Organization and the maintenance schedule optimization became valuable energy saving measure. For adequate implementation of this measure, the accurate prediction of the effects of biofouling on the hydrodynamic characteristics is required. Although computational fluid dynamics approach, based on the modified wall function approach, has imposed itself as one of the most promising tools for this prediction, it requires significant computational time. However, during the maintenance schedule optimization, it is important to rapidly predict the effect of biofouling on the ship hydrodynamic performance. In this paper, the effect of biofilm on the ship hydrodynamic performance is studied using the proposed performance prediction method for three merchant ships. The applicability of this method in the assessment of the effect of biofilm on the ship hydrodynamic performance is demonstrated by comparison of the obtained results using the proposed performance prediction method and computational fluid dynamics approach. The comparison has shown that the highest relative deviation is lower than 4.2% for all propulsion characteristics, lower than 1.5% for propeller rotation rate and lower than 5.2% for delivered power. Thus, a practical tool for the estimation of the effect of biofouling with lower fouling severity on the ship hydrodynamic performance is developed.

1. Introduction

The effect of surface roughness on the ship hydrodynamic performance has been studied for almost 150 years ever since the first Froude tests related to the frictional resistance of smooth and rough flat plates. The assessment of this effect is important as it can provide insights related to benefits of hull cleaning or blasting and re-coating of ship hull. Munk (2006) has estimated that only one third of the world fleet has good coating condition with less than 20% roughness penalty in comparison with smooth surface (Bertram, 2011). The accurate determination of the effect of fouling on the ship hydrodynamic performance is needful for the adequate choice of antifouling (AF) coatings as well as planning of hull cleaning (Uzun et al., 2019). Historical overview of the studies related to investigations of roughness effects on the hydrodynamic performance of ship is presented in (Townsin, 2003). In the beginning of research related to this topic, hull fouling and corrosion were often seen as the same problem. The development of anticorrosive coatings has directed research towards the investigations related to fouling penalties. Namely, biofouling occurrence causes the significant increase in the surface roughness (Seok and Park, 2020a). With the invention of self-polishing coatings based on tributyltin (TBT), the research has been redirected towards the investigation associated with the effect of coating roughness on the ship hydrodynamic performance. Lately, as coatings based on TBT are banned (Farkas et al., 2018b), researchers once again started to study the effect of hull fouling on the ship performance. The most common approach for modelling the effects of surface roughness on the ship hydrodynamic performance is through the application of a certain roughness function (ΔU^+), which represents a downward velocity shift in the Turbulent Boundary Layer (TBL) (Howell and Behrends, 2006). Since there is

* Corresponding author.
E-mail address: nastia.degiuli@fsb.hr (N. Degiuli).
Peer review under responsibility of The Society of Naval Architects of Korea.

https://doi.org/10.1016/j.ijnaoe.2020.12.005

no universal ΔU^+ (Murphy et al., 2018), drag characterization study for certain fouling or roughness type should be performed firstly. Once the relation between ΔU^+ and roughness Reynolds number (k^+) has been determined, it can be utilised for the prediction of frictional drag of any arbitrary body covered with that particular roughness or fouling type (Granville, 1987). Historically, the effect of roughness or biofouling on the ship hydrodynamic performance has been investigated using the Granville similarity law scaling method (Uzun et al., 2020; Demirel et al., 2017b, 2019; Schultz, 2004, 2007). As claimed in (Demirel et al., 2017a) this scaling method has several drawbacks and one of them is that it only allows the assessment of roughness or fouling effects on the frictional resistance of a ship. Recently, researchers have started to use Computational Fluid Dynamics (CFD) approach for the prediction of the roughness effects on the ship hydrodynamic performance. The studies based on CFD approach have several advantages over the Granville similarity law scaling method, since CFD can simulate this phenomenon using the fully non-linear method. Therefore, CFD approach can take into account non-uniform distribution of friction velocity (U_τ) and in that way k^+ as well. On the other hand, the Granville similarity law scaling method can take into account only one k^+ value across the whole immersed surface. In addition, even more significant benefit of CFD approach is that it allows the determination of the roughness effect on each resistance, open water and self-propulsion characteristic (Farkas et al., 2020d). However, Patel (1998) claimed that the most complex problems for CFD are flows at full-scale Reynolds number which take into account surface roughness. Due to complex geometry of biofouling it is impossible to make an actual representation of biofouling within CFD simulation. Nevertheless, if drag characterization of rough surface is known, ΔU^+ model can be either used for the implementation within wall function or to change turbulence boundary conditions in the CFD software (Patel, 1998). Most of the studies investigated the roughness effects on the ship hydrodynamic performance using sand grain roughness approach (Date and Turnock, 1999; Castro et al., 2011; Vargas and Shan, 2016; Seok and Park, 2020b). However, very recently researchers started to employ ΔU^+ models, which are more appropriate for real engineering surfaces, based on the drag characterization studies (Demirel et al., 2014, 2017a; Farkas et al., 2018b, 2020a, 2020b, 2020f; Song et al., 2019, 2020a; Speranza et al., 2019; Andresson et al., 2020). Even though there are alternative methods for modelling the hull roughness within CFD, which are either based on the modification of boundary conditions (Ohashi, 2020) or geometrical resolving the rough surface geometry, due to their limitations (Andresson et al., 2020) the wall function approach has been imposed as the mostly applied one. Thus, the CFD approach based on the modified wall function approach enables the assessment of the effect of biofouling on the resistance, open water and self-propulsion characteristics. Song et al. (2020c) have demonstrated that this approach can accurately predict the effect of roughness on the skin friction, as well as the total resistance of a 3D hull.

Throughout the past several decades, International Towing Tank Conference (ITTC) has followed the investigations associated with the effect of surface roughness on the ship hydrodynamic performance. ITTC takes into account roughness effects on the ship hydrodynamic performance through roughness allowance. Within ITTC 1978 Performance Prediction Method (PPM), roughness allowance is defined with Bowden and Davidson equation (ITTC, 1978). Regardless the fact that this equation has been criticized and challenged immediately after its adoption, it remained in ITTC PPM until 1990, when it was replaced with Townsin and Dey equation (ITTC, 1990). During 26th ITTC meeting, more attention to this problem was given by assembling a Special Committee on Surface Treatment. This committee (ITTC, 2011) has advised researchers to develop new formulae or methods based on the experimental data for the determination of the effect of biofouling on ship resistance and propulsion characteristics. Kresic and Haskell (1983) have proposed the method for estimation of ship and propeller performance in service, i.e. for deteriorated hull and propeller surface condition. Although Kresic and Haskell method for the prediction of the roughness effect on the ship hydrodynamic performance is very important, it allows this assessment only if total roughness height is known. Unfortunately, the determination of roughness height, which could be used as hull roughness and propeller roughness, requires hydrodynamic measurements, as various roughness types have different ΔU^+ models and simple measurement of fouling height is not sufficient. Until new formulae or method is proposed, ITTC (2011) still recommends using Townsin and Dey equation for the roughness allowance, since it is the most suitable option for the time being. This equation can be applied for the determination of frictional resistance coefficient of fouled surface as well, if hydrodynamic tests are performed, i.e. the equivalent sand grain roughness height of certain fouled surface is determined. As performing hydrodynamic tests is quite demanding, one of the recommendations of (ITTC, 2011) is to establish an extensive database of skin friction measurements. Even though the CFD approach currently represents the most comprehensive method for the prediction of the effect of biofouling on the ship hydrodynamic performance, it may be challenging for less experienced users to perform such an investigation (Demirel et al., 2019). In addition to, CFD simulations require significant computational effort, as well as certain time for pre-processing and post-processing. During the maintenance schedule optimization, it is important to rapidly predict the effect of biofouling on the ship hydrodynamic performance. Thus, Oliveira et al. (2020) proposed the use of equivalent sand grain roughness height (k_s) and ΔU^+ model developed in (Demirel et al., 2017a) as a novel performance indicator within ISO 19030 approach for performance monitoring (ISO, 2016). This enabled comparison between ships, increased accuracy for comparison of a ship to itself over time and determination of penalties under operating conditions which differ from past data. However, Oliveira et al. (2020) have assumed that the increases in effective and delivered power are the same, i.e. that the effect of biofouling on the quasi propulsion efficiency is negligible. As shown within (Song et al., 2020a; Farkas et al., 2020f), the increase in delivered power is considerably higher than the increase in effective power if both hull and propeller are fouled. Even if propeller is not fouled, wake field around fouled ship will differ from smooth ship and therefore propeller will operate at different advance coefficient. Thus, the assumption that the increases in effective and delivered power are the same may lead to certain errors. Therefore, robust and reliable PPM for fouled surfaces, which could predict the increase in delivered power would be beneficial. Namely, rapid assessment of the fouling penalty on the delivered power is enabled using this method. This is of particular importance for the assessment of adequate timing for cleaning, since the most important barrier in possible energy savings from the optimized ship maintenance schedule, are lack of information related to the potential benefits and impact of the cleaning on the ship resistance and propulsion characteristics (Farkas et al., 2020b).

In this paper, the effect of biofilm on the ship hydrodynamic performance is studied for three merchant ships using the CFD approach and PPM. The main goal of this study is to demonstrate the applicability of the proposed PPM in the assessment of the effect of biofilm on the ship hydrodynamic performance. Namely, the proposed PPM allows rapid assessment of this effect. The CFD approach presents current state of the art in this field. In order to

demonstrate the applicability, CFD results obtained for smooth surface condition are used as input data for both CFD approach and PPM. Namely, CFD has developed significantly as a tool for the assessment of ship performance (ITTC, 2017). Also, CFD baselines are the most appropriate for fulfilment of the high requirements of ISO performance monitoring standard (ISO, 2016) and therefore CFD is explicitly allowed for obtaining power-speed-draught-trim database for specific ship within procedure for performance monitoring described in ISO 19030 (Kauffeldt and Hansen, 2018). In order to demonstrate the applicability, previously proposed ΔU^+ models for biofilm (Farkas et al., 2018b) are utilised to assess this effect. Also, the ΔU^+ models are implemented within wall function of CFD software in order to simulate the effect of biofilm on the resistance, open water and self-propulsion characteristics. The verification study has been performed and numerical uncertainty has been estimated. The obtained hydrodynamic characteristics for three ships and propellers with smooth surface conditions were validated by comparison with the experimental results (Farkas et al., 2020c). Thereafter, CFD simulations are performed under various fouling conditions and the effect of biofilm on the resistance, open water and self-propulsion characteristics is analysed in detail. Finally, the obtained results using PPM and CFD approach are compared and the comparison has proven the applicability of PPM for fouled surface, thus allowing rapid and satisfactory accurate prediction of the effect of biofouling on the ship hydrodynamic performance. In that way, ITTC (2011) recommendation regarding the proposal of the method, which can account for biofilm effects is fulfilled, and the effects of biofilm on the ship hydrodynamic performance are adequately accounted.

2. Method

2.1. Roughness functions for biofilm

The presence of biofilm on the immersed surfaces causes the decrease in the mean velocity profile within the log-law region of TBL and this downward shift is defined with ΔU^+. ΔU^+ model depicts ΔU^+ values as a function of k^+ which is defined as:

$$k^+ = \frac{kU_\tau}{\nu} \tag{1}$$

where k is the roughness length scale and ν is the kinematic viscosity.

Hydrodynamic tests are required for the determination of k with the aim to find a relation between k and some easily measured surface properties (Monty et al., 2016). Schultz et al. (2015) have proposed a new effective k for fouling with biofilm as follows:

$$k_{eff} = 0.055k\sqrt{\%SC} \tag{2}$$

where k is the average biofilm height and $\%SC$ is the percentage of surface covered with biofilm.

The impact of biofilm on the ship hydrodynamic performance is assessed using three ΔU^+ models proposed in (Farkas et al., 2018b) depending on $\%SC$:

- for $\%SC>25\%$:

$$\Delta U^+ = \begin{cases} \frac{1}{\kappa}\ln(0.27767k^+) & \text{for } k^+ \geq 3.61 \\ 0 & \text{for } k^+ < 3.61 \end{cases} \tag{3}$$

- for $10\%<\%SC<25\%$:

$$\Delta U^+ = \begin{cases} \frac{1}{\kappa}\ln(1.14492 + 0.0988k^+) & \text{for } k^+ \geq 4.5 \\ 0 & \text{for } k^+ < 4.5 \end{cases} \tag{4}$$

- for $\%SC<10\%$:

$$\Delta U^+ = \begin{cases} \frac{1}{\kappa}\ln(1.06492 + 0.05332k^+) & \text{for } k^+ \geq 4 \\ 0 & \text{for } k^+ < 4 \end{cases} \tag{5}$$

where κ is von Karman constant equal to 0.42.

2.2. Performance prediction method for fouled surfaces

The aim of this paper is to demonstrate the applicability of PPM for fouled surfaces, which enables the rapid prediction of the effect of biofouling or roughness on the ship hydrodynamic performance in calm water. The basis of this method is presented in (Farkas et al., 2020e). However, this method has been slightly modified to enable using CFD results for full-scale smooth ship as an input data.

Total resistance coefficient for fouled or rough full-scale ship is determined as follows:

$$C_{TR} = (1+k)C_{FR} + C_W \tag{6}$$

where k is the form factor, C_W is the wave resistance coefficient and C_{FR} is the frictional resistance coefficient for fouled or rough full-scale ship calculated as follows:

$$C_{FR} = C_{FS} + \Delta C_F \tag{7}$$

where C_{FS} is calculated using ITTC 1957 model-ship correlation line and ΔC_F is determined as:

$$\Delta C_F = C_{F0R} - C_{F0S} \tag{8}$$

where C_{F0R} is the frictional resistance coefficient, for a rough flat plate having the same length as a ship, obtained using the Granville similarity law scaling method and C_{F0S} is the frictional resistance coefficient for a smooth flat plate having the same length as a ship obtained using Schoenherr friction line.

The values of thrust deduction fraction (t) and relative rotative efficiency (η_R) for fouled ship are considered to be the same as the ones obtained in CFD simulations for smooth full-scale ship. Wake fraction for fouled ship (w_R) is determined as follows:

$$w_R = (t + 0.04) + (w_S - t - 0.04)\frac{C_{FR}}{C_{FS}} \tag{9}$$

where w_S is the wake fraction determined from CFD simulations for smooth full-scale ship.

PPM for fouled surfaces (Farkas et al., 2020d) accounts for fouling effects on the propeller performance as follows:

$$K_{TR} = K_{TS} - \Delta K_{TD} - \Delta K_{TL} \tag{10}$$

$$K_{QR} = K_{QS} - \Delta K_{QD} - \Delta K_{QL} \tag{11}$$

Changes in K_T and K_Q as a result of increased drag coefficient (C_D) are estimated as follows:

$$\Delta K_{TD} = -\Delta C_D \cdot 0.3 \cdot \frac{P}{D}\frac{c \cdot Z}{D} \tag{12}$$

$$\Delta K_{QD} = \Delta C_D \cdot 0.25 \cdot \frac{c \cdot Z}{D} \tag{13}$$

Changes in K_T and K_Q as a result of reduced value of lift coefficient (C_L) are accounted as follows:

$$\Delta K_{TL} = \Delta C_L \cdot \frac{c \cdot Z}{D} \cdot \frac{0.733 + 0.132J^2}{\sqrt{1 + 0.18(P/D)^2}} \tag{14}$$

$$\Delta K_{QL} = \Delta C_L \cdot \frac{c \cdot Z}{D} \cdot \frac{0.117 + 0.021J^2}{\sqrt{1 + 0.18(P/D)^2}} \tag{15}$$

where K_{TS} and K_{QS} are thrust and torque coefficients for smooth propeller, P is the propeller pitch, D is the propeller diameter, Z is the number of blades, c is the chord length at radius $0.75R$, t is the maximum thickness at radius $0.75R$, ΔC_D is the change in drag coefficient calculated as a difference between C_D for smooth (C_{DS}) and rough surface (C_{DR}), ΔC_L is the change in lift coefficient calculated as $\Delta C_L = -1.1 \cdot \Delta C_D$. In this paper, K_{TS} and K_{QS} are taken from CFD simulations of open water test for smooth propeller. The roughness effects on the propeller performance are assessed based on the equations proposed in (Kresic and Haskell, 1983). It should be noted that several numerical studies demonstrate the impact of biofouling on K_T and K_Q, which is ascribed to the increase in C_D and decrease in C_L of propeller blades (Owen et al., 2018; Song et al., 2020b; Farkas et al., 2020c, 2020d, 2020f). The important difference between method proposed by Kresic and Haskell (1983) and proposed PPM lies in different estimation of C_{DR}.

C_{DS} is determined according to following equation:

$$C_{DS} = 2\left(1 + \frac{t}{c}\right) C_{FS} \tag{16}$$

where C_{FS} is the frictional resistance coefficient of a flat plate having the same length as c obtained for the resultant velocity of the flow approaching the propeller blade section at $r = 0.75R$ (v_R) in full-scale. It should be noted that C_{DR} is calculated analogously to Eq. (16), only C_{FS} is replaced with C_{FR}, which represents the frictional resistance coefficient of a fouled flat plate having the same length as c obtained for v_R using the Granville similarity law scaling method.

The load of the full-scale propeller for fouled ship is calculated as follows:

$$\frac{K_{TR}}{J^2} = \frac{S}{2D^2} \frac{C_{TR}}{(1-t)(1-w_R)^2} \tag{17}$$

where S is the wetted surface area.

Using the load of the full-scale propeller for fouled ship, the advance coefficient (J) for self-propulsion point of fouled ship and propeller (J_R) are read off from the open water diagram for full-scale fouled propeller. Once J_R has been read off, n_R can be easily calculated and the delivered power for fouled condition is determined as follows:

$$P_{DR} = 2\pi n_R Q_R \tag{18}$$

where Q_R is the propeller torque for the fouled propeller and ship.

As can be seen, PPM for fouled surfaces consists of several numerical operations which may produce numerical errors, if performed manually for each fouling condition, ship and propeller. Therefore, an in-house numerical code is developed to allow robust and fast solution. The developed code requires several input data shown in Table 1. It should be noted that resistance, open water and self-propulsion characteristics presented in Table 1 are taken from CFD simulations of resistance, open water and self-propulsion tests for smooth full-scale ship. However, it should be noted that extrapolated towing tank results can be used as an input data as well. Once all input data is imported the code rapidly determines the resistance, open water and self-propulsion characteristics for required fouling condition using above mentioned equations and the Granville similarity law scaling method. This represents an important advantage over the CFD approach for the assessment of the effect of biofouling on the ship hydrodynamic performance. Namely, either full-scale CFD results or extrapolated towing tank results for smooth surface condition are required for the engine selection during the ship design process and therefore every shipowner usually has these data at his disposal. Using this data along with other input data presented in Table 1, one can estimate the impact of certain fouling condition in a matter of seconds. On the other hand, this estimation using CFD approach requires preparation of several numerical simulations including numerical simulation of resistance, open water and self-propulsion tests, processing of these simulations as well as post-processing after the numerical simulation is finished. If the one wants to determine only the increase in P_D and n due to the presence of certain fouling condition, only numerical simulations of self-propulsion tests can be carried out, but with discretized propeller in order to obtain the impact of fouling on the propeller performance. Even for the experienced user and with powerful workstation, the assessment of the effect of certain fouling condition on the ship hydrodynamic performance using CFD approach would take several days or more.

2.3. CFD approach

CFD approach presents current state of the art in the prediction of fouling effects on the ship hydrodynamic performance using method based on the wall similarity hypothesis. The benefits of this approach are presented in previously published studies (Demirel et al., 2014, 2017). This approach is based on Reynolds Averaged Navier-Stokes (RANS) and averaged continuity equations which read:

$$\frac{\partial\left(\rho\overline{u}_i\right)}{\partial t} + \frac{\partial}{\partial x_j}\left(\rho\overline{u}_i\overline{u}_j + \rho\overline{u_i'u_j'}\right) = -\frac{\partial\overline{p}}{\partial x_i} + \frac{\partial\overline{\tau}_{ij}}{\partial x_j} \tag{19}$$

$$\frac{\partial\left(\rho\overline{u}_i\right)}{\partial x_i} = 0 \tag{20}$$

where $\overline{u}_i$ is the averaged velocity vector, $\rho\overline{u_i'u_j'}$ is the Reynolds stress tensor, $\overline{p}$ is the mean pressure and $\overline{\tau}_{ij}$ is the mean viscous stress tensor.

In order to close Eqs. (19) and (20) in this paper, $k-\omega$ Shear Stress Transport (SST) turbulence model is used. The numerical setup, size and discretization of computational domain, applied time step as well as boundary conditions are the same as in (Farkas et al., 2020f). Thus, governing equations are discretized using finite volume method and solved in segregated manner in a way that the second order upwind scheme is used for convective terms and the first order scheme is utilised for temporal discretization. The applied time step within the numerical simulations is determined according to the ratio of ship length and speed and it is equal to $\frac{L}{200 \cdot V}$. Free surface is modelled using Volume Of Fluid (VOF) method, and possible wave reflections are prevented by applying VOF wave

Table 1
Input data for in-house numerical code.

Data type	
ship and propeller	ship speed (v), waterline length (L_{wl}), S, c, t, D, P and Z
fluid and flow properties	density (ρ), dynamic viscosity coefficient (μ), von Karman constant (κ)
fouling condition of a ship and a propeller	fouling height and percentage of surface coverage, fouling type
resistance characteristics for smooth ship	k, total resistance (R_T), frictional resistance (R_F)
open water characteristics for smooth propeller	K_{TS} and K_{QS} for certain J
self-propulsion characteristics	t, η_R and w_S

damping at the inlet, outlet and side boundaries with the damping length set to L. Within (Farkas et al., 2018a, 2019), $k-\omega$ SST turbulence model is demonstrated as a good compromise between the accuracy and computational time in the problems related to ship hydrodynamics and therefore it is applied within this paper. More details regarding $k-\omega$ SST turbulence model can be found in (Farkas et al., 2018a). Numerical simulations of self-propulsion tests are performed using the body force method. The boundary conditions in numerical simulation of resistance and self-propulsion tests are as follows: velocity inlet is applied at inlet, side, top and bottom boundaries, pressure outlet is applied at outlet boundary and no-slip wall is applied at the hull and rudder surfaces. Since within numerical simulations of resistance test, only half of computational domain is modelled, the symmetry boundary condition is applied at the symmetry plane. Computational domain is discretized using unstructured hexahedral mesh and mesh is refined near the free surface, for capturing Kelvin wake, near the hull and rudder surfaces and within numerical simulations of self-propulsion tests in the area where the virtual disk is located. Furthermore, the near wall mesh is generated with the special care, keeping the y^+ value in the first cell near the wall surface above 50 and k^+ value. Since numerical simulations are performed for full-scale ships, it is justified to have higher y^+ values in the first cells near the wall since the boundary layer of a ship has extended log-law and outer region (Farkas et al., 2020a). Therefore, y^+ values above 150 are usual within the numerical simulations for full-scale ships. The generated grid near the wall for numerical simulation of BC is presented in Fig. 1. From Fig. 1 it is clear that the transition from prism layer cells to the core mesh is made appropriately. The obtained y^+ values in the first cell near the wall for smooth KCS, KVLCC2 and BC are from 50 to 400 (Fig. 2), while for fouled KCS, KVLCC2 and BC with R2 are from 50 to 500 (Fig. 3).

Numerical simulations are stopped once total resistance and thrust became steady, which is achieved once these forces oscillate around averaged value with oscillation amplitude lower than 0.5% of average value (Farkas et al., 2017). It should be noted that results of open water test are taken from (Farkas et al., 2020d). The validation and verification studies of CFD simulations for smooth surface condition are performed in (Farkas et al., 2020c).

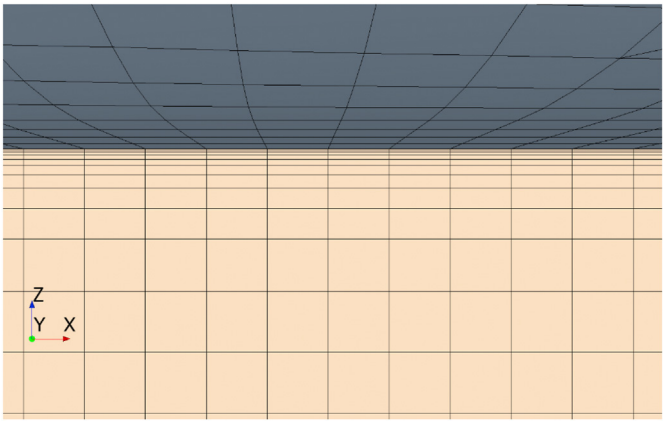

Fig. 1. The near wall mesh for numerical simulation of self-propulsion test of BC.

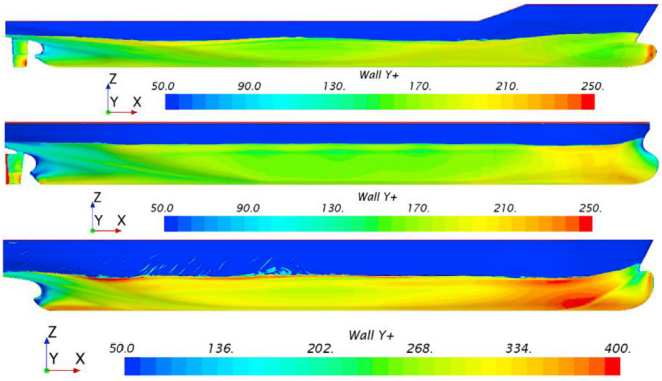

Fig. 2. The obtained y^+ distributions in the first cell near the wall for smooth KCS (upper), KVLCC2 (middle) and BC (lower).

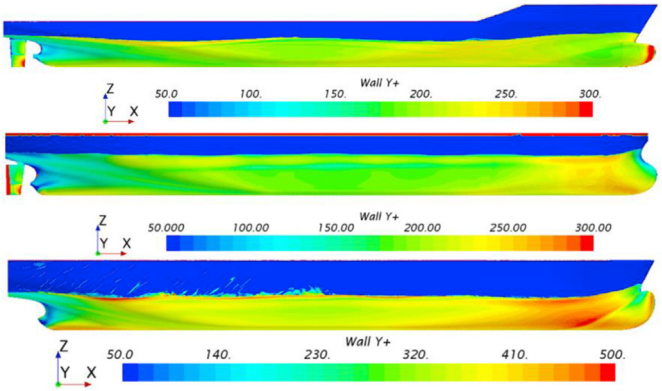

Fig. 3. The obtained y + distributions in the first cell near the wall for KCS (upper), KVLCC2 (middle) and BC (lower) fouled with the surface condition R2.

3. Case study

3.1. Investigated ships and propellers

The applicability of the proposed method is demonstrated for three commercial ships: containership, oil tanker and bulk carrier. KRISO Container Ship (KCS) represents a modern panamax container ship, KRISO Very Large Crude Carrier 2 (KVLCC2) is the typical large oil tanker and Bulk Carrier (BC) is the typical handy-max bulk carrier. The body plans of the investigated ships are

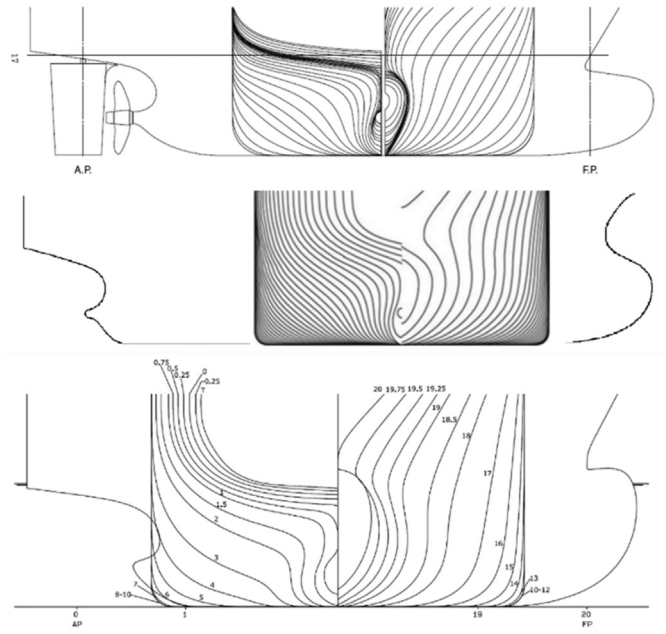

Fig. 4. Body plans of KCS (upper), KVLCC2 (middle) and BC (lower).

Table 2
The main particulars of investigated ships.

Main particular/Ship	KCS	KVLCC2	BC
L_{wl}, m	232.5	325.5	182.69
B, m	32.2	58	30
T, m	10.8	20.8	9.9
Δ, t	53382.8	320750	41755
S, m^2	9645	27467	7351.9
v, kn	24	15.5	16.32
block coefficient, C_B	0.6505	0.8098	0.7834

presented in Fig. 4, while main particulars are presented in Table 2. The investigated ships are equipped with KP505 (KCS), KP458 (KVLCC2) and WB (BC) from Wageningen series. The main particulars of these propellers are presented in Table 3.

3.2. Investigated fouling conditions

The effect of biofilm on the resistance, open water and self-propulsion characteristics is determined using PPM and CFD approach for eight surface conditions presented in Table 4. It should be noted that the same fouling conditions are studied in (Farkas et al., 2018b, 2020b, 2020f) and that these fouling conditions are investigated in the way that certain fouling condition occurs both at the hull and propeller.

The change in certain hydrodynamic characteristic is determined by:

Table 3
The main particulars of investigated propellers.

Main particular/Propeller	KP505	KP458	WB
D, m	7.9	9.86	6.199
P, m	7.505	7.085	5.294
c, m	2.844	2.233	1.633
t, m	0.132	0.131	0.168
Z	5	4	4

Table 4
Investigated fouling conditions.

Fouling condition	k, μm	%SC, %	k_{eff}, μm
R1	100	50	39
R2	500	50	195
R3	100	25	27.5
R4	500	25	137.5
R5	100	15	21.3
R6	500	15	106.5
R7	100	5	12.3
R8	500	5	61.5

$$\Delta\varphi = \frac{\varphi_R - \varphi_S}{\varphi_S} \cdot 100\% \tag{21}$$

where φ denotes certain hydrodynamic characteristic, subscript R denotes fouled surface condition and subscript S smooth surface condition.

3.3. Verification study and comparison

The numerical uncertainties (U_{SN}) in the prediction of ship hydrodynamic characteristics are estimated using the grid convergence index (GCI) method. Thus, the verification study is performed by carrying out the CFD simulations with three different grid sizes and time steps. Thereafter, the grid (U_G) and temporal uncertainties (U_T) are determined using GCI method, which can be utilised for this assessment (Tezdogan et al., 2015; Terziev et al., 2018). More details regarding GCI method are presented in (Farkas et al., 2020b, 2020c). The verification study for CFD simulations of resistance tests of KCS and BC was performed in (Farkas et al., 2020b). The obtained U_{SN} in the determination of R_T for both smooth surfaces and surfaces fouled with biofilm were relatively low, i.e. the highest obtained U_{SN} in the determination of R_T was below 2% (Farkas et al., 2020b). The verification study for CFD simulations of open water tests of propellers KP505, KP458 and WB was performed in (Farkas et al., 2020d) for J value around the expected self-propulsion point. It was performed for smooth propellers and propeller fouled with fouling condition R2, Table 4. The obtained U_{SN} in the determination of K_T and K_Q were relatively low and in the line with the previously published studies (Owen et al., 2018; Song et al., 2020b). Thus, the highest U_{SN} in the determination of K_T was below 4.85%, while the highest U_{SN} in the determination of K_Q was below 1.95%. The verification study for CFD simulations of self-propulsion tests of smooth KCS, KVLCC2 and BC was performed in (Farkas et al., 2020c), while the verification study for CFD simulations of self-propulsion tests of KCS fouled with fouling condition R2 was performed in (Farkas et al., 2020f). The obtained U_{SN} in the determination of P_D, n, T and J were below 4.42%, 2.94%, 3.33% and 3.38% for smooth ship, respectively (Farkas et al., 2020c). The obtained U_{SN} for KCS fouled with fouling condition R2 in the determination of P_D, n, T and J were below 0.37%, 1.25%, 3.46% and 1.11% respectively (Farkas et al., 2020f). It has been demonstrated that the implementation of ΔU^+ models for biofilm did not cause any increase in U_{SN} (Farkas et al., 2020b, 2020d, 2020f).

In this paper, the verification study for CFD simulations of self-propulsion tests of KVLCC2 and BC fouled with fouling condition R2 is carried out. The temporal convergence study is performed with fine mesh and three time steps, i.e. $T/50$, $T/100$ and $T/200$. The grid convergence study is performed with fine time step and three different meshes: coarse, medium and fine. Coarse mesh for CFD simulation of self-propulsion test of KVLCC2 had around 1.25 M cells, medium mesh 2.75 M cells and fine mesh 5.25 M cells. Coarse mesh for CFD simulation of self-propulsion test of BC had around

Table 5
The grid convergence study.

P_D						
Ship	φ_3, MW	φ_2, MW	φ_1, MW	φ_{ext}^{21}, MW	GCI_{fine}^{21}, %	U_G, MW
KVLCC2 R2	29.159	24.940	25.057	25.063	0.033	0.008
BC R2	9.933	9.985	9.383	9.325	0.769	0.072
n						
Ship	φ_3, rpm	φ_2, rpm	φ_1, rpm	φ_{ext}^{21}, rpm	GCI_{fine}^{21}, %	U_G, rpm
KVLCC2 R2	79.832	76.695	76.560	76.548	0.019	0.015
BC R2	108.700	108.852	107.074	106.906	0.196	0.210
T						
Ship	φ_3, kN	φ_2, kN	φ_1, kN	φ_{ext}^{21}, kN	GCI_{fine}^{21}, %	U_G, kN
KVLCC2 R2	2963.66	2586.30	2568.93	2556.22	0.619	15.890
BC R2	1024.29	1029.49	984.48	951.57	4.179	41.143
J						
Ship	φ_3	φ_2	φ_1	φ_{ext}^{21}	GCI_{fine}^{21}, %	U_G
KVLCC2 R2	0.3958	0.4116	0.4068	0.3955	3.451	0.0140
BC R2	0.4632	0.4622	0.4711	0.4776	1.723	0.0081

0.95 M cells, medium mesh 2.2 M cells, while fine mesh 5.05 M cells. The obtained results of grid convergence study are presented in Table 5, while the obtained results of temporal convergence study are presented in Table 6. It should be noted that U_G presented in Table 5 are calculated for fine mesh, and U_T presented in Table 6 are calculated for fine time step. Using U_G and U_T values, U_{SN} in the determination of P_D, n, T and J are calculated. The obtained U_{SN} in the determination of P_D for KVLCC2 is equal to 0.969%, while for BC is equal to 0.846% for fouling condition R2. The obtained U_{SN} in the determination of n for KVLCC2 is equal to 3.613%, while for BC is equal to 0.241% for fouling condition R2. The obtained U_{SN} in the determination of T for KVLCC2 is equal to 1.626%, while for BC is equal to 4.254% for fouling condition R2. The obtained U_{SN} in the determination of J for KVLCC2 is equal to 3.462%, while for BC is equal to 3.633% for fouling condition R2.

The validation study for CFD simulations of resistance, open water and self-propulsion test of investigated smooth ships and propellers is presented in (Farkas et al., 2020c). It should be noted that satisfactory agreement between numerical and extrapolated results is obtained for resistance and propulsion characteristics of all three investigated ships. Thus, the highest obtained relative deviations between CFD and extrapolated results for C_T, P_D and n are lower than 4.34%, 5.70% and 1.79%, respectively. Furthermore, relative deviations for all propulsion characteristics are relatively low, i.e. mostly below 5%. The highest relative deviation between numerically obtained propulsion characteristic and extrapolated one is obtained for $1-w$ for BC and it is equal to −7.418%. This was expected, since CFD simulations of self-propulsion tests were performed with body force method, which models propeller effects rather than discretize propeller itself. More details regarding the body force method and the influence of its application in the prediction of propulsion characteristics are discussed and presented in (Farkas et al., 2018a).

The effect of biofilm on the ship performance is determined using CFD approach and PPM for fouled surfaces presented in subsection 2.2. The main goal of this study is to demonstrate the applicability of PPM by comparing the results obtained using PPM and CFD approach, which currently represents the most comprehensive approach for the prediction of the biofouling effects on the ship performance. Relative deviation between the obtained hydrodynamic characteristics using PPM and CFD approach is calculated as follows:

$$RD = \frac{\varphi_{PPM} - \varphi_{CFD}}{\varphi_{CFD}} \cdot 100\% \tag{22}$$

where subscript PPM depicts that hydrodynamic characteristic is obtained using PPM, and subscript CFD depicts that hydrodynamic characteristic is obtained using CFD.

4. Results

In order to demonstrate the applicability of PPM for fouled surfaces, the obtained resistance and propulsion characteristics using PPM and CFD approach are compared for three investigated

Table 6
The temporal convergence study.

P_D						
Ship	φ_3, MW	φ_2, MW	φ_1, MW	φ_{ext}^{21}, MW	GCI_{fine}^{21}, %	U_T, MW
KVLCC2 R2	24.838	24.714	25.057	25.251	0.968	0.243
BC R2	9.452	9.473	9.383	9.357	0.352	0.033
n						
Ship	φ_3, rpm	φ_2, rpm	φ_1, rpm	φ_{ext}^{21}, rpm	GCI_{fine}^{21}, %	U_T, rpm
KVLCC2 R2	76.507	76.190	76.560	78.773	3.613	2.766
BC R2	107.294	107.156	107.074	106.954	0.140	0.150
T						
Ship	φ_3, kN	φ_2, kN	φ_1, kN	φ_{ext}^{21}, kN	GCI_{fine}^{21}, %	U_T, kN
KVLCC2 R2	2585.99	2545.97	2568.93	2599.83	1.504	38.626
BC R2	976.76	981.39	984.48	990.72	0.792	7.801
J						
Ship	φ_3	φ_2	φ_1	φ_{ext}^{21}	GCI_{fine}^{21}, %	U_T
KVLCC2 R2	0.4092	0.4099	0.4068	0.4059	0.277	0.0011
BC R2	0.4706	0.4737	0.4711	0.4591	3.199	0.0151

ships. It should be noted that the applicability of propeller PPM for fouled surfaces is demonstrated within (Farkas et al., 2020d).

The effect of biofilm on ΔP_E,ΔP_D and Δn, obtained using PPM and CFD approach is shown in Figs. 5–7. In Fig. 5, the obtained ΔP_E are shown and it can be concluded that satisfactory agreement between results obtained using PPM and CFD approach is obtained. The obtained ΔP_E are substantial, especially for fouling conditions with higher k_{eff} value. Thus, $\Delta P_E$for KCS range from 0% (PPM) and 0.48% (CFD) for R7 up to 30.62% (PPM) and 25.76% (CFD) for R2, while ΔP_E for KVLCC2 from 0% (PPM) and 0.01% (CFD) for R7 up to 31.52% (PPM) and 27.95% (CFD) for R2 and for BC from 0% (PPM) and 0.70% (CFD) for R7 up to 29.51% (PPM) and 29.36% (CFD) for R2. Although satisfactory agreement between ΔP_E obtained using PPM and CFD approach is obtained, it is clear that the highest discrepancies are obtained for KCS. This can be explained with the fact that KCS has the highest portion of R_W in R_T and since within PPM it is assumed that R_W is not affected due to the presence of fouling, the obtained ΔP_E for KCS are most affected by this assumption. Namely

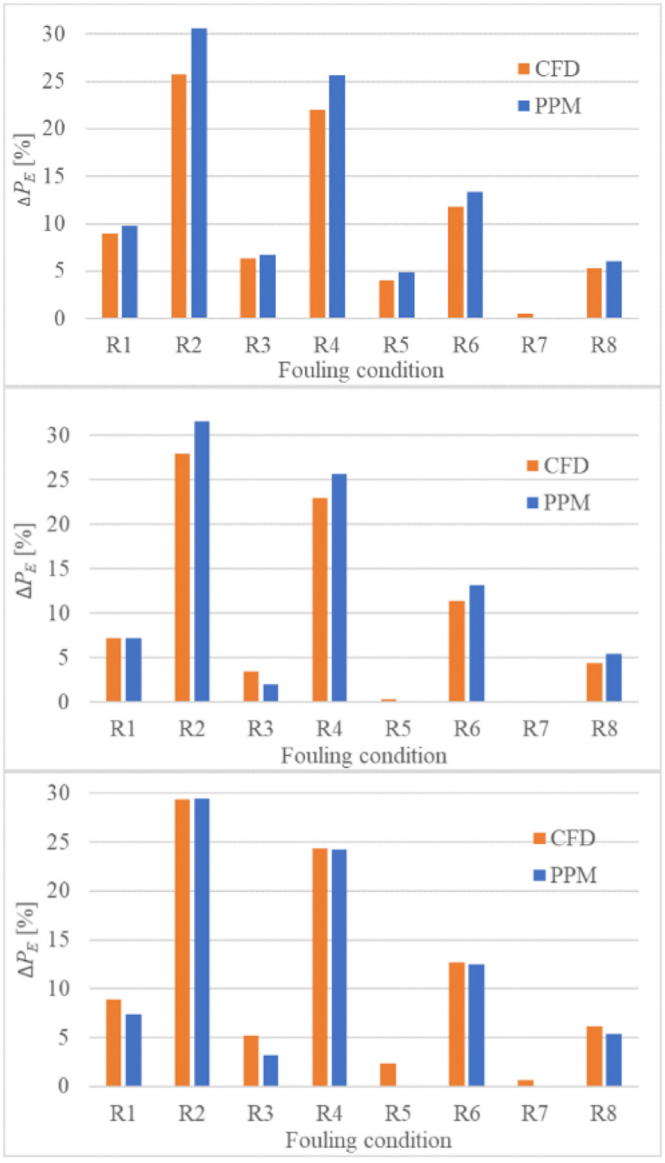

Fig. 5. The obtained effect of biofilm on ΔP_E for KCS (upper), KVLCC2 (middle) and BC (lower).

Fig. 6. The obtained effect of biofilm on ΔP_D for KCS (upper), KVLCC2 (middle) and BC (lower).

as shown in (Song et al., 2019; Farkas et al., 2020a, 2020b; Demirel et al., 2017), the presence of biofouling causes the decrease in R_W. Because of this, R_T predicted using PPM is slightly higher than the one predicted using CFD. More discussion regarding this is presented in section 5. In Fig. 6, the obtained ΔP_D are shown and it can be concluded that satisfactory agreement between the results obtained using PPM and CFD approach is obtained. Thus, ΔP_D for KCS range from 0.89% (PPM) and 1.40% (CFD) for R7 up to 43.44% (PPM) and 36.33% (CFD) for R2, for KVLCC2 from 0.46% (PPM) and 0.36% (CFD) for R7 up to 40.86% (PPM) and 40.38% (CFD) for R2 and for BC from 0.37% (PPM) and 0.41% (CFD) for R7 up to 42.79% (PPM) and 39.53% (CFD) for R2. As for ΔP_E, the highest discrepancies in the prediction of ΔP_D using PPM and CFD approach are obtained for KCS, which can be explained with the fact that the higher R_T leads to higher propeller load, which results in higher prediction of P_D. The obtained Δn are presented in Fig. 7 and for KCS due to the presence of biofilm range from 0.17% (PPM) and 0.12% (CFD) for R7 up to 6.43% (PPM) and 4.85% (CFD) for R2 B, for KVLCC2 from 0.02% (PPM) and 0.09% (CFD) for R7 up to 7.38% (PPM) and 8.05% (CFD) for

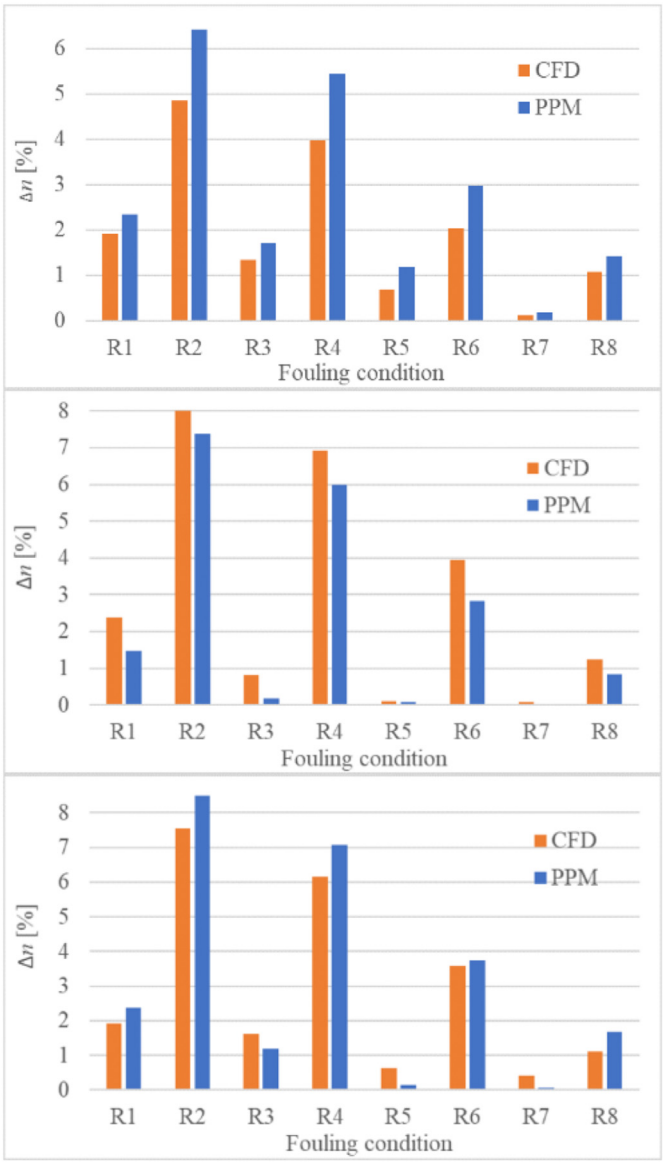

Fig. 7. The obtained effect of biofilm on Δn for KCS (upper), KVLCC2 (middle) and BC (lower).

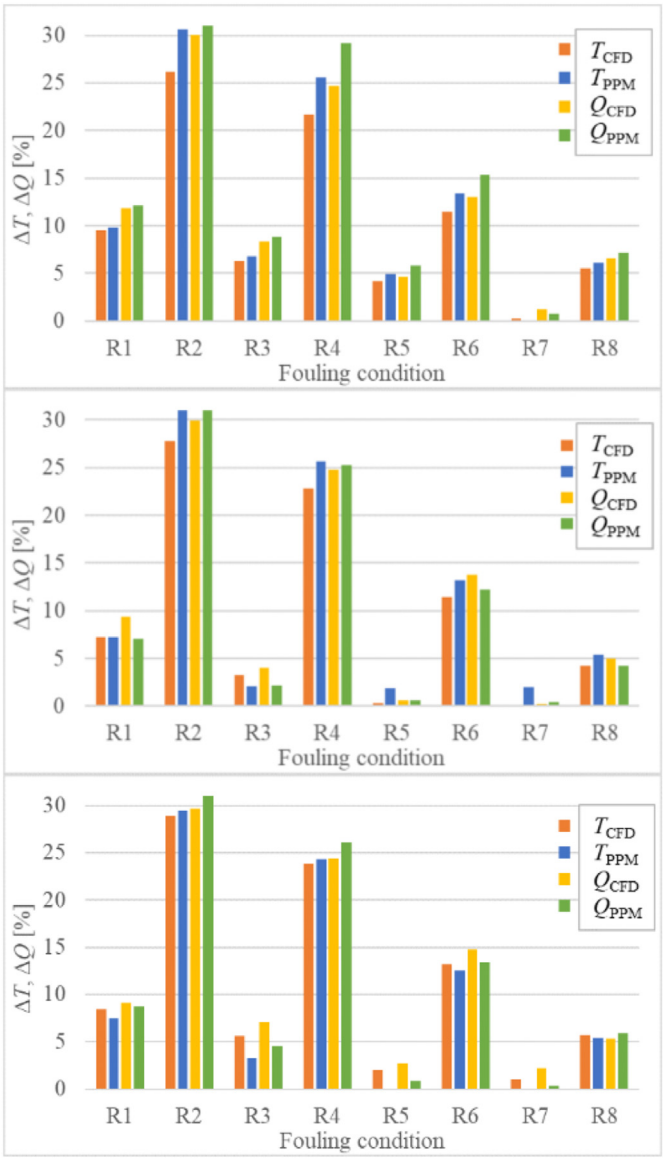

Fig. 8. The obtained effect of biofilm on ΔT and ΔQ for KCS (upper), KVLCC2 (middle) and BC (lower).

R2 and for BC from 0.06% (PPM) and 0.41% (CFD) for R7 up to 8.51% (PPM) and 7.57% (CFD) for R2. The highest discrepancies in the predicted Δn between PPM and CFD approach is obtained for KCS, which was expected as explained earlier.

The proposed PPM can appropriately assess the effect of biofilm on increases in T and Q as well, which is clear from Fig. 8. Thus, the obtained ΔT for KCS range from 0.06% (PPM) and 0.28% (CFD) for R7 up to 30.66% (PPM) and 26.15% (CFD) for R2, for KVLCC2 from 1.88% (PPM) for R5 and 0.07% (CFD) for R7 up to 31.53% (PPM) and 27.83% (CFD) for R2 B and for BC from 0.01% (PPM) for R5 and 1.04% (CFD) for R7 up to 29.52% (PPM) and 28.87% (CFD) for R2. The obtained ΔQ for KCS range from 0.72% (PPM) and 1.27% (CFD) for R7 up to 34.78% (PPM) and 30.02% (CFD) for R2, for KVLCC2 from 0.44% (PPM) and 0.27% (CFD) for R7 up to 31.19% (PPM) and 29.92% (CFD) for R2 and for BC from 0.06% (PPM) and 2.21% (CFD) for R7 up to 31.59% (PPM) and 29.71% (CFD) for R2.

As the applicability of propeller PPM is already demonstrated in (Farkas et al., 2020d), the accuracy of PPM in the assessment of the effect of biofilm on the self-propulsion characteristics is investigated. In Tables 7–9, the obtained self-propulsion characteristics using PPM are shown along with *RD* from CFD results. The obtained self-propulsion characteristics using PPM have very low *RD* from the ones obtained using the CFD approach, which demonstrates the applicability of the proposed method. The proposed method considers that t and η_R are the same for smooth and fouled condition, which was also assumed by Townsin et al. (1985) and obtained in (Farkas et al., 2020f). The obtained *RD* between t and η_R obtained using PPM and CFD are lower than 0.5% for all investigated fouling conditions and ships. The accurate assessment of the self-propulsion point for fouled ship depends on the accurate prediction of J for the self-propulsion point. As can be seen from Tables 7–9, the highest *RD* between J obtained using PPM and CFD for KCS is equal to 0.73%, for KVLCC2 to 1.1% and for BC to 1.77%. It should be noted that the obtained *RD* are lower than the numerical uncertainty in the prediction of J presented in subsection 3.3. Therefore, it can be concluded that PPM has successfully predicted J for the self-propulsion point of fouled ship and propeller. Regarding

Table 7
The obtained self-propulsion characteristics for KCS using PPM.

Propulsion characteristic	R1	R2	R3	R4	R5	R6	R7	R8
$1-t$	0.867	0.867	0.867	0.867	0.867	0.867	0.867	0.867
RD, %	0.43	−0.31	0.12	0.33	−0.10	0.35	0.20	−0.19
$1-w$	0.766	0.751	0.768	0.754	0.769	0.763	0.773	0.768
RD, %	0.43	0.85	0.15	0.68	0.12	0.45	0.06	0.15
η_H	1.132	1.155	1.129	1.149	1.127	1.136	1.122	1.128
RD, %	0.00	−0.53	−0.28	−1.00	−0.02	−0.80	−0.25	0.04
η_O	0.664	0.620	0.672	0.630	0.683	0.660	0.694	0.679
RD, %	−0.12	−0.96	−0.35	−1.25	−0.85	−0.98	−0.12	−0.43
η_B	0.665	0.621	0.673	0.631	0.685	0.661	0.696	0.681
RD, %	0.05	−0.73	−0.11	−1.07	−0.70	−0.80	0.33	−0.26
η_R	1.002	1.002	1.002	1.002	1.002	1.002	1.002	1.002
RD, %	0.17	0.23	0.24	0.19	0.15	0.18	0.45	0.17
η_P	0.753	0.717	0.760	0.725	0.772	0.751	0.780	0.768
RD, %	0.05	−1.26	−0.39	−2.05	−0.72	−1.59	0.08	−0.22
J	0.706	0.666	0.713	0.675	0.718	0.699	0.728	0.715
RD, %	0.01	−0.65	−0.21	−0.73	−0.35	−0.45	0.01	−0.21
K_T	0.173	0.191	0.171	0.187	0.169	0.177	0.165	0.170
RD, %	−0.50	0.52	−0.18	0.38	−0.17	−0.08	−0.32	−0.18
$10K_Q$	0.293	0.325	0.288	0.318	0.283	0.298	0.275	0.285
RD, %	−0.54	0.61	−0.28	0.71	0.19	0.26	−0.65	−0.12

Table 8
The obtained propulsion characteristics for KVLCC2 using PPM.

Propulsion characteristic	R1	R2	R3	R4	R5	R6	R7	R8
$1-t$	0.820	0.820	0.820	0.820	0.820	0.820	0.819	0.820
RD, %	0.04	−0.10	−0.17	−0.04	−0.02	0.02	0.05	−0.16
$1-w$	0.660	0.632	0.666	0.638	0.668	0.653	0.668	0.662
RD, %	−0.33	−1.61	0.29	−1.97	0.01	−0.62	0.01	0.13
η_H	1.243	1.298	1.232	1.284	1.227	1.256	1.227	1.239
RD, %	0.38	1.54	−0.46	1.97	−0.02	0.65	0.04	−0.29
η_O	0.585	0.530	0.597	0.543	0.608	0.575	0.610	0.596
RD, %	2.59	0.87	1.49	0.72	1.83	3.70	1.69	1.89
η_B	0.584	0.529	0.596	0.542	0.607	0.574	0.609	0.595
RD, %	2.77	0.89	1.70	0.75	1.62	3.35	1.85	2.37
η_R	0.998	0.998	0.998	0.998	0.998	0.998	0.998	0.998
RD, %	0.17	0.01	0.20	0.03	−0.20	−0.34	0.16	0.47
η_P	0.726	0.687	0.734	0.696	0.745	0.721	0.747	0.738
RD, %	3.16	2.44	1.23	2.73	1.60	4.03	1.90	2.08
J	0.445	0.403	0.455	0.412	0.457	0.435	0.457	0.449
RD, %	0.58	−1.00	0.94	−1.10	0.03	0.44	0.08	0.53
K_T	0.155	0.170	0.151	0.166	0.151	0.159	0.152	0.154
RD, %	1.87	4.19	0.19	4.09	1.58	3.72	2.09	1.96
$10K_Q$	0.188	0.205	0.184	0.201	0.181	0.191	0.181	0.185
RD, %	−0.30	2.24	−0.56	2.19	−0.01	0.79	0.31	0.13

Table 9
The obtained propulsion characteristics for BC using PPM.

Propulsion characteristic	R1	R2	R3	R4	R5	R6	R7	R8
$1-t$	0.764	0.764	0.764	0.764	0.764	0.764	0.764	0.764
RD, %	−0.43	−0.38	0.38	−0.45	−0.38	0.49	−0.34	−0.42
$1-w$	0.646	0.628	0.650	0.632	0.653	0.642	0.653	0.648
RD, %	0.94	1.09	1.33	1.05	0.61	1.92	1.07	0.42
η_H	1.182	1.218	1.176	1.209	1.171	1.190	1.171	1.179
RD, %	−1.35	−1.45	−0.94	−1.49	−0.98	−1.40	−0.73	−0.84
η_O	0.595	0.543	0.605	0.555	0.616	0.586	0.620	0.605
RD, %	−0.59	−0.65	2.07	−0.69	0.90	2.51	2.33	−1.28
η_B	0.595	0.543	0.605	0.555	0.616	0.586	0.620	0.605
RD, %	−0.15	−0.72	1.91	−0.83	0.98	2.34	2.32	−0.94
η_R	1.000	1.000	1.000	1.000	1.000	1.000	1.000	1.000
RD, %	0.45	−0.08	−0.16	−0.14	0.08	−0.16	−0.01	0.35
η_P	0.703	0.661	0.711	0.671	0.722	0.697	0.726	0.714
RD, %	−1.50	−2.16	0.96	−2.31	−0.01	0.91	1.58	−1.78
J	0.515	0.472	0.524	0.482	0.532	0.505	0.533	0.520
RD, %	0.48	0.21	1.77	0.18	1.09	1.77	1.43	−0.11
K_T	0.188	0.202	0.185	0.199	0.183	0.192	0.183	0.187
RD, %	−1.84	−1.23	−1.39	−1.38	−0.98	−0.89	−0.30	−1.32
$10K_Q$	0.259	0.279	0.255	0.274	0.251	0.263	0.250	0.256
RD, %	−1.22	−0.30	−1.53	−0.38	−0.87	−1.45	−1.17	−0.49

the assessment of $1-w$ and η_H, it can be seen from Tables 7–9 that satisfactory agreement between the results obtained using PPM and CFD approach is obtained as well. Thus, the highest *RD* between $1-w$ obtained using PPM and CFD for KCS is equal to 0.85%, for KVLCC2 to 1.97% and for BC to 1.92%, while the highest *RD* between η_H obtained using PPM and CFD for KCS is equal to 1%, for KVLCC2 to 1.97% and for BC to 1.49%. The assessment of η_O and η_B within PPM depends on the accurate assessment of propeller load defined with Eq. (17) and fouled propeller performance in open water conditions. Namely, once the propeller load has been determined, the intersection with $K_T = f(J)$ from open water test could be found. This intersection defines J, K_T and K_Q for open water condition ($K_{Q,\ OWT}$) values. As can be seen from Table 7, the obtained η_O, η_B, K_T and $10K_Q$ values for KCS using PPM are almost the same as the ones obtained using CFD. Thus, the highest *RD* between η_O obtained using the newly proposed PPM and CFD is equal to 1.25%, for η_B to 1.07%, for K_T to 0.52%, while for $10K_Q$ to 0.71%. It should be noted that slightly higher *RD* between the obtained η_O, η_B, K_T and $10K_Q$ values using PPM and CFD approach are obtained for KVLCC2 and BC, however those *RD* are also relatively low. Thus, the highest *RD* between η_O obtained using PPM and CFD is equal to 3.70%, for η_B to 3.35%, for K_T to 4.19%, for $10K_Q$ to 2.24% for KVLCC2, while for BC the highest *RD* for η_O is equal to 2.51%, for η_B to 2.34%, for K_T to 1.84%, while for $10K_Q$ to 1.53%. Finally, it can be concluded that PPM has successfully predicted η_P of fouled ship and propeller. Namely, the highest *RD* between η_P obtained using the newly proposed PPM and CFD for KCS is equal to 2.05%, for KVLCC2 to 4.03% and for BC to 2.31%.

5. Discussion

For ship owners or ship operators it is crucial to determine the economic aspect of implementing certain operational measure once considering the improvement of ship energy efficiency. Since biofouling represents an important problem, which causes the increase in fuel consumption, or reduction in ship speed, it reduces the ship energy efficiency. The maintenance schedule optimization represents a valuable operational measure over which ship owner or ship operator has a large degree of control and for successful implementation of such measure the assessment of the effects of biofouling on the ship performance are valuable. During the maintenance schedule optimization economic aspect is crucial, i.e. ship owner or ship operator will decide to clean ship and propeller if the costs of cleaning are economically justified. Since cleaning cannot be performed while sailing, but in port or in dry dock, it is important to estimate whether it is economically justified to clean a ship and/or propeller. Obviously, it is important to make such an assessment rapidly, since whenever ship does not operate, its owner or operator does not make money. In the investigation regarding the economic aspect of cleaning, numerous costs must be considered. The benefits of cleaning will be achieved through the reduction of fuel consumption, i.e. the fuel costs will be lower, which is very important since fuel costs represent 60–70% of the entire operational costs (Park et al., 2018). Therefore, the accurate assessment of the fuel savings related to hull and propeller cleaning enables the accurate assessment of economic aspects regarding the implementation of such operational measure. The CFD approach based on the implementation of ΔU^+ model within the wall function has imposed itself as one of the most promising tools for this prediction. However, the important shortcomings of the CFD approach are that it requires significant amount of calculation time and that user must have certain experience in its application. The proposed PPM has enabled rapid and accurate assessment of resistance, open water and self-propulsion characteristics of fouled ship. The applicability of the newly proposed method is demonstrated in section 4 for three merchant ships. The most important parameters in the prediction of fuel consumption are related to the propeller operating point, i.e. P_D and n. The obtained P_D and n using PPM and CFD approach for eight investigated fouling conditions and for three ships are presented in Tables 10 and 11, along with the obtained *RD*.

From Table 10 it can be seen that the obtained P_D using PPM have very low *RD* from the obtained P_D using the CFD approach. Thus, the highest *RD* between $P_{D,\ \mathrm{PPM}}$ and $P_{D,\ \mathrm{CFD}}$ for KCS is equal to 5.22%, for KVLCC2 to −2.99% and for BC to −2.78%. The obtained *RD* between n_{PPM} and n_{CFD} are even lower and for KCS the highest *RD* is equal to 1.51%, for KVLCC2 to −0.91% and for BC to 0.88%. Therefore, it can be concluded that detrimental effects of biofilm on the ship hydrodynamic performance can be accurately predicted using PPM. The important benefit of the proposed method is that it can be utilised for various ships, as well as for various fouling conditions defined with certain ΔU^+ model. Furthermore, the impact of cleaning solely the propeller or ship hull on the ship hydrodynamic performance can be investigated as well. This represents an important benefit over the performance monitoring methods, which are usually used for the determination of the effect of biofouling on the ship performance nowadays. Namely, it is very difficult to separate the effect of biofouling on the hull and propeller once performance monitoring methods are used (van Ballegooijen and Helsloot, 2019). However, it is important to note that this method is more suitable for the prediction of the fouling effects on the ship performance for fouling with lower fouling severity because of two reasons. The first reason is that within PPM it is assumed that R_W is the same for smooth and fouled ship. While the effect of fouling on R_W is moderate for fouling with lower fouling severity, this effect is significantly higher for fouling with higher fouling severity, such as hard fouling, as presented in (Farkas et al., 2020a). Since it has been shown that the presence of fouling causes the decrease in R_W, the proposed PPM will predict too high R_T in a case of fouling with higher fouling severity. Consequently, the propeller load will be too high and J for the self-propulsion point will not be adequately predicted. The effect of biofouling on R_W is more important for ships which sail at higher *Fn*, i.e. for the ships which have higher portion of R_W in R_T. Because of this the highest *RD* between $P_{D,\ \mathrm{PPM}}$ and $P_{D,\ \mathrm{CFD}}$ is achieved for KCS for fouling conditions R2 and R4, which represent conditions with the highest k_{eff}, Table 4. Therefore, it can be concluded that the proposed PPM is the most accurate for fouling conditions with lower fouling severity and ships with higher portion of R_V in R_T. Mentioned drawback can be overcome with the correction of C_W due to the presence of biofouling, i.e. roughness. In order to estimate this correction, several other studies regarding the effect of biofouling or roughness on R_W for various ships must be performed. Additional reason for the inaccurate prediction of the fouling effects on the ship performance in the case of higher fouling severity lies in the inaccurate prediction of C_{F0R} using the Granville similarity law scaling method. Namely, as presented in (Farkas et al., 2020a), higher *RD* between C_{F0R} obtained using CFD approach and the Granville similarity law scaling method are obtained for hard fouling than biofilm (Farkas et al., 2018b). This can be attributed to the fact that only one value of k^+ is assumed once the Granville method is used, which means that only one ΔU^+ value is used along the whole flat plate. For the proposed method the accurate prediction of C_{F0R} is of utmost importance, since C_{F0R} is utilised for the prediction of R_{TR}, w_R and therefore the propeller load as well. Since the flat plate simulation requires relatively low computational effort, especially in comparison with full-scale self-propulsion tests, mentioned drawback can be overcome with those

Table 10
The obtained P_D using the newly proposed PPM and CFD approach.

Ship	KCS		KVLCC2		BC	
Fouling condition	$P_{D,\ CFD}$, MW	$P_{D,\ PPM}$, MW *RD*, %	$P_{D,\ CFD}$, MW	$P_{D,\ PPM}$, MW *RD*, %	$P_{D,\ CFD}$, MW	$P_{D,\ PPM}$, MW *RD*, %
R1	28.063	28.262 0.71	19.988	19.390 −2.99	7.476	7.487 0.15
R2	33.569	35.321 5.22	25.057	25.144 0.35	9.383	9.602 2.34
R3	27.030	27.248 0.81	18.727	18.264 −2.48	7.319	7.115 −2.78
R4	31.932	33.552 5.07	23.815	23.697 −0.50	8.877	9.078 2.26
R5	25.940	26.357 1.60	17.988	17.974 −0.08	6.950	6.792 −2.27
R6	28.405	29.261 3.02	21.106	20.607 −2.37	7.995	7.914 −1.01
R7	24.968	24.843 −0.50	17.913	17.932 0.10	6.902	6.750 −2.21
R8	26.518	26.771 0.95	18.975	18.769 −1.09	7.160	7.240 1.12

Table 11
The obtained n using the newly proposed PPM and CFD approach.

Ship	KCS		KVLCC2		BC	
Fouling condition	n_{CFD}, rpm	n_{PPM}, rpm *RD*, %	n_{CFD}, rpm	n_{PPM}, rpm *RD*, %	n_{CFD}, rpm	n_{PPM}, rpm *RD*, %
R1	101.242	101.663 0.42	72.550	71.890 −0.91	101.436	101.905 0.46
R2	104.159	105.727 1.51	76.560	76.084 −0.62	107.074	108.008 0.87
R3	100.672	101.036 0.36	71.440	70.978 −0.65	101.144	100.713 −0.43
R4	103.288	104.758 1.42	75.762	75.092 −0.88	105.662	106.588 0.88
R5	100.035	100.505 0.47	70.927	70.911 −0.02	100.166	99.692 −0.47
R6	101.374	102.293 0.91	73.646	72.869 −1.05	103.113	103.264 0.15
R7	99.462	99.511 0.05	70.919	70.869 −0.07	99.950	99.598 −0.35
R8	100.404	100.762 0.36	71.741	71.449 −0.41	100.655	101.193 0.53

numerical simulations, i.e. that C_{F0R} is obtained from the numerical simulations of flat plate. If so, the assessment of the effect of hard fouling on the performance of KVLCC2 using the newly proposed PPM would probably be more accurate, since the portion of R_W in R_T for KVLCC2 is negligible.

Therefore, in order to investigate the applicability of the newly proposed PPM for different fouling type and ship, two aspects must be analysed. The first is that the portion of R_W in R_T for the investigated ship must be moderate and the second one is the accuracy of the Granville similarity law scaling method in the prediction of C_{F0R}.

It is important to note that in case of higher fouling severity on the immersed surface, the ship owner or ship operator will decide to clean ship or propeller, since the fouling penalties are too high, as presented in (Farkas et al., 2020c). Therefore, it is more important to determine a proper time to clean ship or propeller for fouling with lower fouling severity, i.e. before the occurrence of hard fouling, which will result in high fuel penalties. The newly proposed method can be valuable tool for the determination of the effect of such fouling condition on the ship hydrodynamic performance.

6. Conclusion and future work

This study demonstrated the applicability of the proposed PPM in the assessment of the effect of biofilm on the ship hydrodynamic performance. This was done by comparing the obtained resistance and propulsion characteristics of three ships fouled with eight different fouling conditions using PPM and CFD approach. Namely, the proposed PPM allows rapid assessment of the effect of biofouling on the ship hydrodynamic performance and CFD approach presents current state of the art in this field. The comparison proved the applicability of PPM, thus allowing rapid and satisfactory accurate determination of the effect of biofouling on the ship hydrodynamic performance. In that way, ITTC (ITTC, 2011) recommendation regarding the proposal of the method, which can account for biofilm effects, was fulfilled, and the effects of biofilm on the ship hydrodynamic performance were adequately accounted. It should be noted that the newly proposed method is applicable to various ships and fouling types and enables a rapid assessment of fouling penalties. Finally, it can be a practical tool during the maintenance schedule optimization for the estimation of the effect of biofouling with lower fouling severity on the ship hydrodynamic performance.

Since during the voyage added resistance in waves will occur, future work will be focused on including these effects within PPM. This would enable a more accurate assessment of potential energy savings related to fuel oil consumption and CO_2 emission due to the hull and propeller cleaning. Thus, more reliable data for the

economic analysis of the ship and propeller cleaning would be enabled as well, which represents the most important barrier in the maintenance schedule optimization. In order to increase the accuracy of the proposed PPM, future studies will be focused on the drawbacks mentioned in the discussion. Thus, additional investigations related to the effect of biofouling or roughness on R_W for various ships will be performed and the correction of C_W due to the presence of biofouling, i.e. roughness will be proposed. For more severe fouling conditions, C_{FOR} obtained from the numerical simulations of flat plate will be used for the prediction of fouling effect on the ship hydrodynamic performance. In that way a more reliable assessment of the effect of more severe fouling condition will be enabled.

Declaration of competing interest

The authors declare that they have no known competing financial interests or personal relationships that could have appeared to influence the work reported in this paper.

References

Andersson, J., Oliveira, D.R., Yeginbayeva, I., Leer-Andersen, M., Bensow, R.E., 2020. Review and comparison of methods to model ship hull roughness. Appl. Ocean Res. 99, 102119.

Bertram, V., 2011. Practical Ship Hydrodynamics, second ed. Elsevier, Amsterdam, Netherland.

Castro, A.M., Carrica, P.M., Stern, F., 2011. Full scale self-propulsion computations using discretized propeller for the KRISO container ship KCS. Comput. Fluid 51 (1), 35–47.

Date, J.C., Turnock, S.R. (1999). A study into the techniques needed to accurately predict skin friction using RANS solvers with validation against Froude's historical flat plate experimental data. Report.

Demirel, Y.K., Khorasanchi, M., Turan, O., Incecik, A., Schultz, M.P., 2014. A CFD model for the frictional resistance prediction of antifouling coatings. Ocean. Eng. 89, 21–31.

Demirel, Y.K., Turan, O., Incecik, A., 2017a. Predicting the effect of biofouling on ship resistance using CFD. Appl. Ocean Res. 62, 100–118.

Demirel, Y.K., Uzun, D., Zhang, Y., Fang, H.C., Day, A.H., Turan, O., 2017b. Effect of barnacle fouling on ship resistance and powering. Biofouling 33 (10), 819–834.

Demirel, Y.K., Song, S., Turan, O., Incecik, A., 2019. Practical added resistance diagrams to predict fouling impact on ship performance. Ocean. Eng. 186, 106112.

Farkas, A., Degiuli, N., Martić, I., 2017. Numerical investigation into the interaction of resistance components for a series 60 catamaran. Ocean. Eng. 146, 151–169.

Farkas, A., Degiuli, N., Martić, I., 2018a. Assessment of hydrodynamic characteristics of a full-scale ship at different draughts. Ocean. Eng. 156, 135–152.

Farkas, A., Degiuli, N., Martić, I., 2018b. Towards the prediction of the effect of biofilm on the ship resistance using CFD. Ocean. Eng. 167, 169–186.

Farkas, A., Degiuli, N., Martić, I., Dejhalla, R., 2019. Numerical and experimental assessment of nominal wake for a bulk carrier. J. Mar. Sci. Technol. 24 (4), 1092–1104.

Farkas, A., Degiuli, N., Martić, I., 2020a. An investigation into the effect of hard fouling on the ship resistance using CFD. Appl. Ocean Res. 100, 102205.

Farkas, A., Degiuli, N., Martić, I., 2020b. Impact of biofilm on the resistance characteristics and nominal wake. Proc. IME M J. Eng. Marit. Environ. 234 (1), 59–75.

Farkas, A., Degiuli, N., Martić, I., Dejhalla, R., 2020c. Impact of hard fouling on the ship performance of different ship forms. J. Mar. Sci. Eng. 8 (10), 748.

Farkas, A., Degiuli, N., Martić, I., 2020d. The impact of biofouling on the propeller performance. Ocean. Eng. 219, 108376.

Farkas, A., Degiuli, N., Martić, I., Ančić, I., 2020e. Performance prediction method for fouled surfaces. Appl. Ocean Res. 99, 102151.

Farkas, A., Song, S., Degiuli, N., Martić, I., Demirel, Y.K., 2020f. Impact of biofilm on the ship propulsion characteristics and the speed reduction. Ocean. Eng. 199, 107033.

Granville, P.S., 1987. Three indirect methods for the drag characterization of arbitrarily rough surfaces on flat plates. J. Ship Res. 31, 70–77.

Howell, D., Behrends, B., 2006. A review of surface roughness in antifouling coatings illustrating the importance of cutoff length. Biofouling 22 (6), 401–410.

International Organization for Standardization (ISO), 2016. ISO 19030-1:2016 Ships and Marine Technology-Measurement of Changes in Hull and Propeller Performance-Part 1: General Principles.

ITTC, 1990. Report of the powering performance committee. Proceedings of the 19th ITTC.

ITTC Recommended Procedures and Guidelines, 1978. 1978 ITTC Performance Prediction Method.

ITTC Specialist Committee on Performance of Ships in Service, 2017. Final report and recommendation to the 28th ITTC. In: Proceedings of 28th ITTC, vol. II. Wuxi, China.

ITTC Specialist Committee on Surface Treatment, 2011. Final report and recommendation to the 26th ITTC. In: Proceedings of 26th ITTC, vol. II.

Kauffeldt, A., Hansen, H., 2018. Enhanced performance analysis and benchmarking with CFD baselines. In: Bertram, V. (Ed.), 3rd Hull Performance & Insight Conference -HullPIC'18; Redworth, UK, 12-14 March 2018.

Krešić, M., Haskell, B., 1983. Effects of propeller design-point definition on the performance of a propeller/diesel engine system with regard to in-service roughness and weather conditions. SNAME Transactions 91, 195–224.

Monty, J.P., Dogan, E., Hanson, R., Scardino, A.J., Ganapathisubramani, B., Hutchins, N., 2016. An assessment of the ship drag penalty arising from light calcareous tubeworm fouling. Biofouling 32 (4), 451–464.

Murphy, E.A., Barros, J.M., Schultz, M.P., Flack, K.A., Steppe, C.N., Reidenbach, M.A., 2018. Roughness effects of diatomaceous slime fouling on turbulent boundary layer hydrodynamics. Biofouling 34 (9), 976–988.

Ohashi, K., 2020. Numerical study of roughness model effect including low-Reynolds number model and wall function method at actual ship scale. J. Mar. Sci. Technol. 1–13.

Oliveira, D.R., Granhag, L., Larsson, L., 2020. A novel indicator for ship hull and propeller performance: examples from two shipping segments. Ocean. Eng. 205, 107229.

Owen, D., Demirel, Y.K., Oguz, E., Tezdogan, T., Incecik, A., 2018. Investigating the effect of biofouling on propeller characteristics using CFD. Ocean. Eng. 159, 505–516.

Park, J., Kim, B., Shim, H., Ahn, K., Park, J.H., Jeong, D., Jeong, S., 2018. Hull and propeller fouling decomposition and its prediction based on machine learning approach. In: Bertram, V. (Ed.), 3rd Hull Performance & Insight Conference -HullPIC'18, vol. 12, pp. 20–26.

Patel, V.C., 1998. Perspective: flow at high Reynolds number and over rough surfaces—achilles heel of CFD. J. Fluid Eng. 120, 434–444.

Schultz, M.P., 2004. Frictional resistance of antifouling coating systems. J. Fluid Eng. 126 (6), 1039–1047.

Schultz, M.P., 2007. Effects of coating roughness and biofouling on ship resistance and powering. Biofouling 23 (5), 331–341.

Schultz, M.P., Walker, J.M., Steppe, C.N., Flack, K.A., 2015. Impact of diatomaceous biofilms on the frictional drag of fouling-release coatings. Biofouling 31 (9–10), 759–773.

Seok, J., Park, J.C., 2020a. A fundamental study on measurement of hull roughness. Brodogradnja: Teorija i praksa brodogradnje i pomorske tehnike 71 (1), 59–69.

Seok, J., Park, J.C., 2020b. Numerical simulation of resistance performance according to surface roughness in container ships. International Journal of Naval Architecture and Ocean Engineering 12, 11–19.

Song, S., Demirel, Y.K., Atlar, M., 2019. An investigation into the effect of biofouling on the ship hydrodynamic characteristics using CFD. Ocean. Eng. 175, 122–137.

Song, S., Demirel, Y.K., Atlar, M., 2020a. Penalty of hull and propeller fouling on ship self-propulsion performance. Appl. Ocean Res. 94, 102006.

Song, S., Demirel, Y.K., Atlar, M., 2020b. Propeller performance penalty of biofouling: computational fluid dynamics prediction. J. Offshore Mech. Arctic Eng. 142 (6), 061901.

Song, S., Demirel, Y.K., Atlar, M., Dai, S., Day, S., Turan, O., 2020c. Validation of the CFD approach for modelling roughness effect on ship resistance. Ocean. Eng. 200, 107029.

Speranza, N., Kidd, B., Schultz, M.P., Viola, I.M., 2019. Modelling of hull roughness. Ocean. Eng. 174, 31–42.

Terziev, M., Tezdogan, T., Oguz, E., Gourlay, T., Demirel, Y.K., Incecik, A., 2018. Numerical investigation of the behaviour and performance of ships advancing through restricted shallow waters. J. Fluid Struct. 76, 185–215.

Tezdogan, T., Demirel, Y.K., Kellett, P., Khorasanchi, M., Incecik, A., Turan, O., 2015. Full-scale unsteady RANS CFD simulations of ship behaviour and performance in head seas due to slow steaming. Ocean. Eng. 97, 186–206.

Townsin, R.L., 2003. The ship hull fouling penalty. Biofouling 19 (S1), 9–15.

Townsin, R.L., Spencer, D.S., Mosaad, M., 1985. Rough propeller penalties. Trans. - Soc. Nav. Archit. Mar. Eng. 93, 165–187.

Uzun, D., Demirel, Y.K., Coraddu, A., Turan, O., 2019. Time-dependent biofouling growth model for predicting the effects of biofouling on ship resistance and powering. Ocean. Eng. 191, 106432.

Uzun, D., Ozyurt, R., Demirel, Y.K., Turan, O., 2020. Does the barnacle settlement pattern affect ship resistance and powering? Appl. Ocean Res. 95, 102020.

van Ballegooijen, E., Helsloot, T., 2019. An approach to monitor the propeller separately from the hull. In: Bertram, V. (Ed.), 4th Hull Performance & Insight Conference -HullPIC'19; Gubbio, Italy, 6-8 May 2019., pp. 50–55.

Vargas, A., Shan, H., 2016. A numerical approach for modelling roughness for marine applications. In: Proceedings of the ASME 2016 Fluids Engineering Division Summer Meeting FEDSM2016. Washington, USA, 10-14 July 2016.